Surface Characterization of Thin Titanium Foils Processed by Femtosecond Laser Ablation in Liquids

Philipp L. Maack*[1], Christian R. Günther[1], Konrad Bargon[1], Alexander Kanitz[2], Cemal Esen[1], and Andreas Ostendorf[1]

[1]*Applied Laser Technologies, Ruhr University Bochum, Universitätsstraße 150, D-44801 Bochum, Germany*
[2]*Lidrotec GmbH, Lothringer Allee 2, D-44805 Bochum, Germany*
**Corresponding author's e-mail: philipp.maack@ruhr-uni-bochum.de*

Laser ablation in liquids offers some key advantages over conventional laser processing under gaseous or inert conditions. A significant volumetric reduction of the heat affected zone minimizes the risk of damaging adjacent regions during processing. Due to complex physicochemical interactions the interactions in the ablation zone and their impact need to be investigated. For this study, titanium was chosen as a base material, as it is widely used in a broad range of micromachining applications. The results of the change of ablation rate, surface roughness and surface oxidation for thin titanium foils in both purified water and argon are presented and compared respectively. Processing in the much denser liquid medium reveals differences in the fluence dependant ablation characteristics and an overall reduction in the ablation rate, supposedly caused by plasma-shielding. Favourable aspects are given by the higher surface quality and improved dimensional tolerances, making the process a promising alternative in micromachining applications.
DOI: 10.2961/jlmn.2024.01.2001
Keywords: titanium, laser ablation, liquids, surface roughness, SEM, LSM, EDX

1. Introduction

Ultrashort pulsed laser ablation is a process, commonly used in industrial applications and research for precision micromachining of metals [1, 2], semiconductors [3, 4], and ceramics [5]. Laser ablation in liquid-phase (LAL) is a modified variant that was initially used towards the end of the 20th century to generate nanoparticles by incubating the ablated matter within the confined ablation plume, surrounded by a dense plasma [6]. The extreme physicochemical conditions within the spatially confined ablation plume, are characterized temporally by high temperature and pressure gradients. The liquid environment affects the ablation process in different ways, compared to processing in a gaseous environment. While heat conduction into the base material is negligible for ultrashort pulsed laser processing in general, ejection of superheated debris into a thin atmosphere is prone to recondensation of ablated matter and thus contamination of adjacent regions. Time-consuming post-processing can be reduced by using LAL, since the significantly increased thermal conductivity of the much denser liquid media cause almost instantaneous solidification of the ejected matter. Thus, a direct enhancement in surface-quality can be obtained solely by changing the processing medium. However, LAL may also be impeded by temporally overlapping effects between two subsequent ultrashort laser pulses, and nonlinear effects at elevated intensities, such as plasma-shielding and self-focusing, concurrent to the pulse duration [7]. Those nonlinear effects manifest in distinctive ablation characteristics, such as fluctuating ablation rates, mainly as a function of applied fluence, surrounding medium and material-type. Apart from exotic ablation techniques, like water-jet coupled laser beams [8], light propagation through stationary or flowing liquid films is the common practice. However, controlling the fluid is an inherently challenging task, subdivided into open- or closed fluid-film configuration with constant or variable film-thickness [9]. Regarding the liquids themselves, there is a great potential to benefit from unique physical and chemical reactions, such as the correlation between bubble expansion and surface tension, diffusion processes and surface oxidation. However, using highly reactive media can increase the risk of excessive corrosion or even potentially dangerous characteristics, such as toxicity and flammability. In the case of micromachining of delicate structures without further modifications, using purified water as the liquid medium is sufficient, since it offers excellent surface quality at the best availability.

2. Methods and Materials

In this study surface and sub-surface modification by femtosecond laser ablation of thin titanium foils, submerged within flowing purified water with an electric conductivity of $\sigma \approx 3\ \mu S\ cm^{-1}$, and under a constant flow of argon (Air Liquide Alphagaz 1 Ar 99.999 %) are investigated. For all experiments $20\ mm \times 20\ mm$ strips of $125\ \mu m$ thick grade 1 titanium, cut from the same metal sheet, were used. The beam of a diode pumped femtosecond disk laser (JENOPTIK JenLas D2.fs) was expanded to a diameter of 6 mm and collimated into a laserscanning head (Scanlab SCANcube III 10). Subsequent deflection and focusing through the integrated 63 mm non-telecentric f-theta-lens (Scanlab 116213) ensures dynamic positioning within a broad fluence range. Optical distortions were minimized by scanning only within the ablation areas of $200\ \mu m \times 200\ \mu m$, while coarse positioning between ablation areas was performed via movement of separate motorized mechanical axis. The laser´s wavelength $\lambda_0 = 1030\ nm$, pulse frequency $f_{pulse} = 200$ kHz and pulse duration $t_{pulse} = 400$ fs were held constant. The

calibrated average power at the target was varied between $P_{avg} = 0.1 - 2.4\,\mathrm{W}$ and measured with a power meter (Coherent PowerMax PM30) before each experiment. Fig. 1 shows a cross-sectional view of the process chamber with two different configurations (a) for gas and (b) for liquids, used for all experiments.

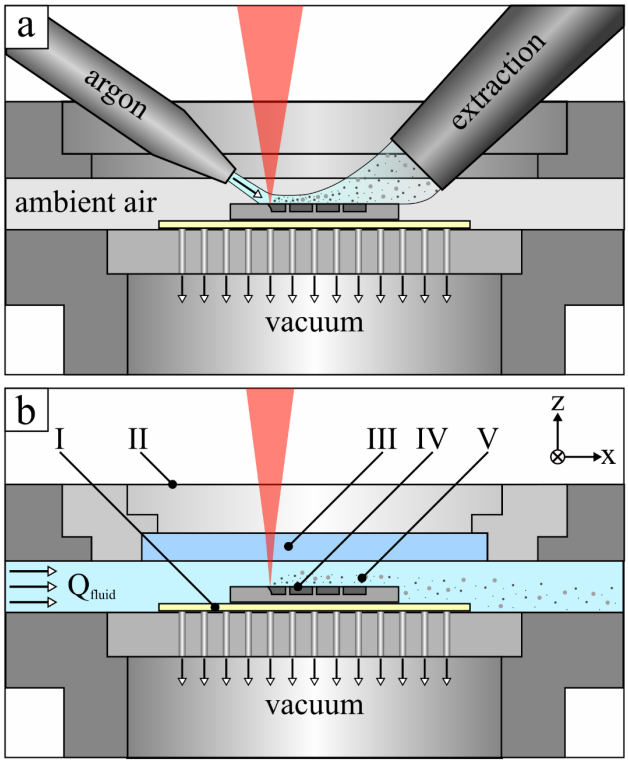

Fig. 1 Cross-sectional view of the processing chamber, (a) with a gas nozzle and vacuum extraction, or (b) as a closed configuration for laser ablation in liquids with a sealed lid (II) and integrated laser window (III). The thin titanium foil sticks to a flexible carrier (I), which is securely held in place by an integrated vacuum-table. Ablated debris (V) from irradiated areas (IV) is (b) carried away and subsequently filtered in a secondary water system or (a) extracted by vacuum.

In both cases, the flexible sample carrier is securely held in place on a vacuum chuck, that is integrated in a self-developed processing chamber. For LAL the chamber is closed above the sample carrier with a sealed lid. In the center of the lid, an anti-reflection (AR) coated laser window made from fused silica is embedded. The bottom side of the window is parallel to the foil´s surface and held at a constant distance, depending on its thickness. For all tests, the volumetric flow was set to the maximum available rate of flow, measured at $10.5\,\mathrm{l\,min^{-1}}$ which is corresponding to an average flow velocity of approximately $760\ \mathrm{mm\,s^{-1}}$, under the assumption of a uniform flow field. Due to their minuscule thermal mass, most of the ablated particles are rapidly cooled down by the surrounding liquid, without the risk of recondensation and sticking to the substrate´s surface. Continuous filtering of the colloids in a secondary cycle further minimizes contamination in the closed loop fluidic system. In addition, water in the primary cycle is replaced by purified water prior to each experiment, to lower the risk of cross-contamination from other experiments. Laser irradiation under gaseous conditions was conducted without the sealed lid, to prevent the AR coating of the laser window from getting substantially damaged by superheated ablation particles. To guarantee a good removal of recondensed particles a high constant gas flow of about $25\,\mathrm{l\,min^{-1}}$ was applied to the irradiated surface, using a flat shaped nozzle of $1\,\mathrm{mm} \times 12\,\mathrm{mm}$. Since argon and air share almost identical refractive indices at the laser wavelength λ_0, changes of the focal plane are considered negligible.

Scanning electron microscope (SEM) images were obtained using a ZEISS EVO MA 10, with an integrated Bruker Quantax XFlash Detector 410-M, for energy dispersive X-ray spectroscopy (EDX) measurements. Acquisition of volumetric data and surface roughness values from ablated areas was acquired through laser scanning microscopy, using an Olympus LEXT 3D Measuring Laser Microscope OLS5000-SAF with an LMPlanFL N 50x objective. For specialized measurements in the experimental determination of beam waist radii, standard light microscopy was performed using a Nikon ECLIPSE LV100.

3. Light-Matter-Interaction

During laser irradiation of the titanium foils photons that are not reflected from the surface get absorbed within the skin layer of the metal, also called optical penetration depth.

$$\delta = \sqrt{\frac{2\rho}{2\pi f \mu_0 \mu_r}};\ \mu_0 = 1.256 \cdot 10^{-6}\,\mathrm{NA^{-2}} \tag{1}$$

$$\rho_{Ti} = 4.2 \cdot 10^{-7}\ \Omega\mathrm{m};\ f_{\lambda_0} = 2.913\ \mathrm{s^{-1}};\ \mu_{r,\mathrm{Ti}} \approx 1 \tag{2}$$

According to equation (1) and constants (2), the penetration depth for titanium at the given laser wavelength $\lambda = cf$ is approximated to $\delta_{Ti} \approx 19\,\mathrm{nm}$, where c is the propagation velocity of the electromagnetic wave, f is the frequency of the electromagnetic wave, ρ is the resistivity of the medium, μ_r is the relative permeability of the medium and μ_0 is the permeability of free space. The photons absorbed by free electrons within the conduction band increase their potential energy. As a result, the electrons reach subsequent thermalization of the electron gas on the timescale of femtosecond under the assumption of linear absorption and the fluences given in this study. Final heating of the lattice structure by energy transfer from electrons is comparably slow, taking several picoseconds before temperature equalization between electrons and phonons. Due to the large difference between the timescales for excitation and energy transfer, varying pulse durations below a few hundred femtoseconds have little influence on the process.

Within the near infrared (NIR) band, strong light absorption effects need to be considered when the light is propagating through a liquid medium. For a constant attenuation factor α along the propagation distance z, the light absorption within a thin water layer between the bottom of the glass and the sample's surface can be described by the Lambert-Beer law for a linear absorption behavior.

$$I(z) = I_0 \exp(-\alpha z);\ \alpha = 2\kappa\omega c^{-1} \tag{3}$$

$$\kappa_{H_2O} = 1.659 \cdot 10^{-6} \quad [10] \tag{4}$$

According to equation (3) and the extinction coefficient κ_{H_2O} for water (4), the calculated energy absorption is estimated to be around 4.5 %, where c is the propagation

velocity of the electromagnetic wave and ω is its angular frequency. In combination with a transmission of 99.6 % for the AR coated glass, the total estimated absorption equals 4.9 %. For a more precise adjustment of the values, the actual absorption within the glass and the water layer have been measured as a function of different fluences. The estimated and measured values are in good correspondence, whereas a correction by a more precise interpolation between measured points has been chosen for all following measurements over a single calculated correction factor.

3.1 Self-focusing

In addition to the light attenuation, a different beam divergency for the propagation in water can be expected, incorporating intensity variations. According to Snell's law (5), the beam parameter product (6) and case specific constants (7), the focused laser beam is shifting to greater angles of refraction θ_2 at the air-glass interface and again to lower angles of refraction at the glass-water interface of the laser window, causing a downward shift of the focal plane and a decreased beam waist ω_0. With the geometrical constants for the laser-window and water-film thickness, the shift of the focal plane is calculated to $\Delta z_f \approx 1.49\,\mathrm{mm}$, which is in great accordance with experimental measurements at low intensities. The calculated beam waist radii for focusing within argon and water respectively are listed in Table 1.

$$n_1 \sin\theta_1 = n_2 \sin\theta_2 \tag{5}$$

$$\omega_0 = M^2 \lambda \pi^{-1} \varphi^{-1} \tag{6}$$

$$n_{air} \approx 1; n_{SiO_2} \approx 1.45\,; \mathrm{n_{H_2O}} \approx 1.33 \tag{7}$$

$$M^2 = 1.25\,; f = 63\,\mathrm{mm}\,; \lambda_0 = 1030\,\mathrm{nm}$$

Considering only linear refraction is sufficient for a general understanding of the beam propagation, however there is a great discrepancy between the calculated and actual parameters when compared to real experiments. A more precise approach can be achieved by experimental approximation of the beam waist radius for a Gaussian intensity distribution, proposed by Liu et al. [11]. According to his findings, the gradient ρ of a logarithmic spline (8) within a semi-log plot for different r^2 over Φ_0, where r are the radii for distinctive phase-transitions of amorphous rings of a (111) silicon-crystal surface irradiated at different fluences Φ_0, are proportional to the beam waist radius $\omega_0 \sim \sqrt{2}\rho$.

$$r^2 = \rho^2\left(\ln \Phi_0 - \ln \Phi_{r_0}\right) \tag{8}$$

This method is not only independent from the distance between the plane of measurement to the actual focal plane, but also from an absolute precision for the fluence Φ_0. The fluence is derived from relative power readings, which makes its results favourable over the estimated parameters used in equation (6). For metals, the radii of the distinctive ablation boundaries can be used instead of phase transition rings.

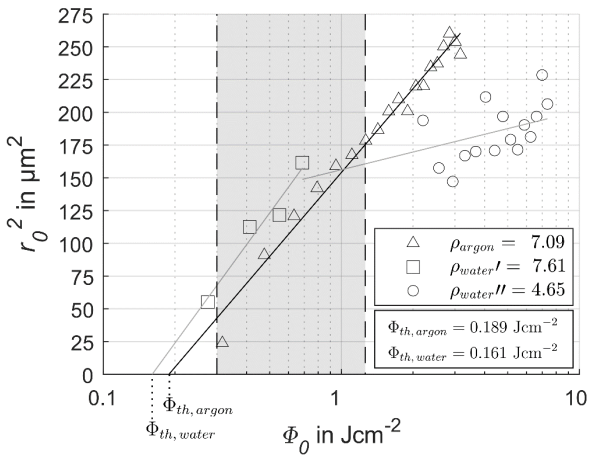

Fig. 2 Experimental determination of the beam waist radius ω_0 (cf. Table 1), derived from the spline gradient ρ within a semi-log plot of $r_0{}^2$ as a function of fluence Φ_0. The different radii r_0 of distinctive concentric markings on the surface of a titanium foil were measured, using a confocal microscope. Self-focusing within water is indicated by a change in the gray splines' gradients. The gray window indicates the range for the expected start of self-focusing within water.

Fig. 2 shows two semi-log plots according to Liu's method, for processing of a titanium foil under a constant flow of argon (△) and for processing in purified water (□, ○). For processing within gas, uniformly distributed measurements around one single logarithmic spline (black line, △) indicate a linear beam propagation, independent from the applied fluence or pulse energy. While this context is true for most applications under gaseous conditions, ultrashort laser pulses with sufficient pulse energy that propagate through a much denser solid or liquid medium oftentimes exceeded the critical pulse power P_{crit} (9), thus inducing self-focusing.

$$P_{crit} = \frac{\alpha {\lambda_0}^2}{8\pi n_0 n_2}\,;\ \alpha = 3.77\,;\ \lambda_0 = 1030\,\mathrm{nm} \tag{9}$$

This nonlinear behavior, known as optical Kerr effect, is caused by a change of the material´s refractive index, due to its energy dependent complex part in $n = n_r + I(r,z,t)n_i$, where n_r and n_i stand for the linear and nonlinear refractive indices, r and z being radial and axial coordinates for the beam expansion and t the time constant. Although literature values for n_2 are subject to considerable variations, according to (9) and [12] the critical pulse power threshold for self-focusing within water can be estimated to be around $2.9 - 4.3$ MW, which is equivalent to $0.3 - 1.26$ Jcm^{-2} in this work (Fig. 2 – gray region). For a peak pulse power below the critical threshold for self-focusing within water, converted to around $0.7\,\mathrm{Jcm^{-2}}$, the initial gradient $\rho_{H_2O}{}'$ (gray line, □) is slightly larger than ρ_{Ar}. This indicates the expected expansion of the beam waist from linear refraction at the glass-water interface, satisfying Snell's law. However, with increasing fluence, the gradient (gray line, ○) declines rapidly, confirming the initial assumption of a nonlinear beam propagation within water. Although a single gradient over a wide fluence range above Φ_{crit} does only give a vague approximation, it must be considered over a linear approach. In this work, the measurements are adjusted

according to the spline gradients from Fig. 2 with their respective beam waist radii listed in Table 1.

Table 1 Determined beam waist radii ω_0 for processing within argon and within water, as a function of fluence. Two different methods were used, one considering the beam parameter product and aperture changes trough refraction at the glass-water interface of the laser window (Snellius) and the other experimental determined beam radii values at different fluences (Liu).

medium	fluence range	ω_0 $(Snellius)$	ω_0 (Liu)
argon	$0 - 3.0\ \mathrm{J/cm^2}$	8.6 µm	10.03 µm
water	$0 - 0.7\ \mathrm{J/cm^2}$	11.4 µm	10.77 µm
	$0.7 - 8\ \mathrm{J/cm^2}$		6.58 µm

4. Results

Laser ablation within gas and laser ablation within liquid are based on the same physical principles, which are fundamentally described in section 3. However, the processing media chosen in this study give rise to initially unexpected phenomena during laser irradiation of titanium substrates. Due to their different nature of interaction with this metal, the experimental results and their underlying physical principles will be discussed separately in terms of their ablation characteristics, followed by the discussion of the collective surface characterization and a conclusion.

4.1 Ablation – Titanium in argon

Argon was chosen as a process gas, as it is commonly used in research and development, as well as industrial applications due to its easy availability. Moreover, its inert properties and thus inability to form chemical bonds with other elements, are key aspects for laser-based micromachining with high pulse fluences.

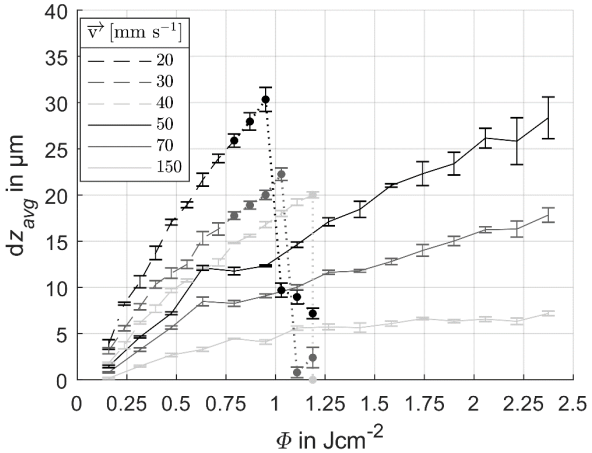

Fig. 3 Average ablation depth $\mathrm{d}z_{avg}$, acquired from laser scanning measurements after laser ablation of titanium under a constant flow of argon, as a function of fluence Φ and scanning speed $\vec{v}$. The average ablation depth gradually increases for higher fluences and lower scanning speeds, before plasma-shielding, defocusing, and self-focusing effects induce sub-surface ablation. Manual delamination of impeding surface layers during post-processed cleaning enabled measurements of additional points (dashed lines: ●) in subsequent measurements.

Fig. 3 shows the mean ablation depth $\mathrm{d}z_{avg}$ as a function of fluence Φ and scanning speed $\vec{v}$. Each point corresponds to the arithmetic mean of three subsequent laser-scanning measurements taken in the centre of an irradiated area of $200\ \mu\mathrm{m} \times 200\ \mu\mathrm{m}$ on the surface of a thin titanium foil. The same strategy was applied for all areas, with scanning and gas flow directions opposite to each other and a constant hatching distance of $\Delta h = 5\ \mu\mathrm{m}$ with one single pass per line and area.

The scanning speed was gradually increased from $10\ \mathrm{mm\,s^{-1}}$ to $150\ \mathrm{mm\,s^{-1}}$ in equally spaced increments for a total of 15 different datasets, corresponding to a very high pulse overlapping factors, ranging from 96.26 % to 99.75 %, derived from equations used by Schnell et al. [13] for femtosecond surface structuring of Ti6Al4V. To improve readability only a few measurements are displayed in Fig. 3. As expected for laser ablation of metal substrates within a gaseous environment, the ablation depth increases with a higher accumulated fluence dose Φ_{dose}, describing the total energy input per area. Different combinations of applied fluence and scanning speed determine the accumulative fluence. For combinations that exceed a threshold of around $35\ \mathrm{kJcm^{-2}}$ the ablation depth unexpectedly declines to values near zero (cf. Fig. 3, dashed lines: ●). Fig. 4 shows SEM images of three different areas after irradiation with different fluence doses (a – b). While for a relatively low fluence dose (a) no abnormality can be observed, an increased (c1 – c3) or even extreme fluence dose (b1, b2) is accompanied with drastic changes to the surface structure and roughness.

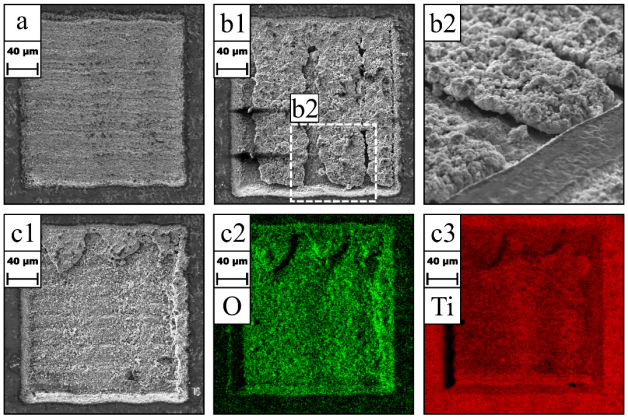

Fig. 4 SEM images and EDX measurements taken from irradiated titanium after laser ablation under a constant flow of argon. Different applied fluences, of (a) $0.16\ \mathrm{Jcm^{-2}}$, (b) $0.79\ \mathrm{Jcm^{-2}}$, and (c) $0.63\ \mathrm{Jcm^{-2}}$, show the formation of free-floating structures (b2), which can be assigned to titanium oxides (c2: 66.67 At. - % oxygen, c3: 33.33 At. - % titanium). Strong surface oxidation indicates that ambient air is drawn into the process gas stream. SEM imaging (a, b, c1) was conducted at an acceleration voltage of 10 kV and a current of 600 pA, while EDX measurements (c2, c3) correspond to 20 kV and 50 pA for a duration of 60 minutes at approximately 3600 counts per second.

Changing from a top view to a tilted observation angle (b2), indicates that the formations are loosely interconnected, free-floating structures. An early approach to explain this phenomenon as deposition of remelted particles was dismissed, since there are no significant changes for different scanning directions in relation to the gas flow and the flow rate. Additionally, the same phenomenon could be observed irrespective of the area's dimensions. Comparative ablation tests with pressurized air and under low vacuum

indicate a connection between the formation of the observed structures and a reduced presence of atmospheric oxygen during processing. EDX measurements (c2, c3) for irradiation with a medium fluence dose (c1) under argon reveals a significant presence of oxygen within the irradiated area, supposedly originating from ambient air drawn into the process gas stream. According to the relative atomic mass distribution, the chemical composition can be assigned mainly to titanium dioxide (TiO_2), whereas non-stoichiometric titanium sub oxides might also be involved.

Semi-transparent optical properties of titanium-based oxides are well-known for interferometric colouring through thermal laser marking by nanosecond lasers [14], so that the assumption of high light transmittance and subsequent below-surface focusing under the presence of titanium oxides is made here. A great example with comparable changes to the surface of an yttria-stabilized zirconia ceramic (YSZ), with similar optical properties, is given by Kiel et al. [15]. In his work, the selective delamination of thin ceramic layers upon processing with a femtosecond laser of identical wavelength and comparable fluences is reported. Depending on the overlap, applied power and repetition rate, delamination starting below 5 $\mathrm{Jcm^{-2}}$ and little to no influence on the ablation depth as a function of total energy dose is reported. Aside from a lower fluence threshold for delamination, minor variations in the ablation depth can also be observed for titanium, as shown in figure Fig. 5.

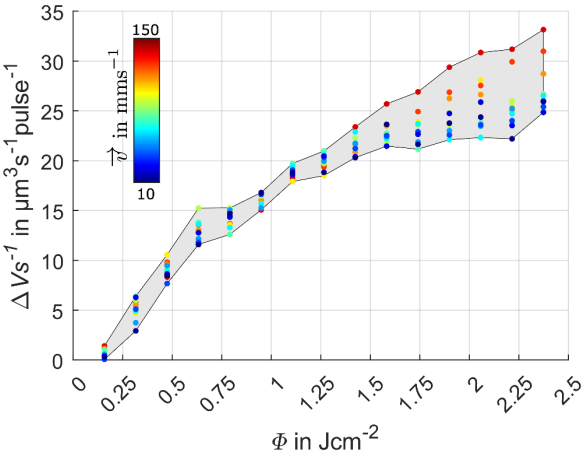

Fig. 5 Volumetric ablation per second / ablation efficiency for laser ablation of titanium under a constant flow of argon, as a function of fluence Φ. A slight increase in ablation efficiency for higher scanning speeds is observed, especially at higher fluences. Measurements below 50 mm $\mathrm{s^{-1}}$ were discarded, due to their tendency to form oxide layers that are prone to delamination (cf. Fig. 3).

In contrast to the experiments for the already semi-transparent YSZ, a surface layer of titanium oxides is not present initially, so that at low fluences non-reflected photons are solely absorbed within the skin layer of the metal. With increasing fluence, gradual formation of titanium oxides is observed. It is assumed, that the formation of a high-density plasma from free electrons of the electron gas and ablated particles is involved, which in turn lowers the effective energy through plasma shielding. Additionally, antiwaveguiding / defocusing effects, may also lower the effective fluence at the surface drastically, thus impeding the ablation process. Instead, wave propagation through the new semitransparent oxide layers could experience strong self-focusing deep below the surface. This is also indicated by a very low critical power for self-focusing in TiO_2 bulk material, which is calculated to 0.1 MW by equation (9). This research is experimentally supported by the investigations of the change in ablation depths for surface and sub-surface laser ablation, using a laser scanning microscope. Fig. 6 shows a selection of different applied fluences (c, d) for a constant scanning speed $\vec{v} = 30$ mm $\mathrm{s^{-1}}$ and repetition rate $f_{pulse} = 200$ kHz.

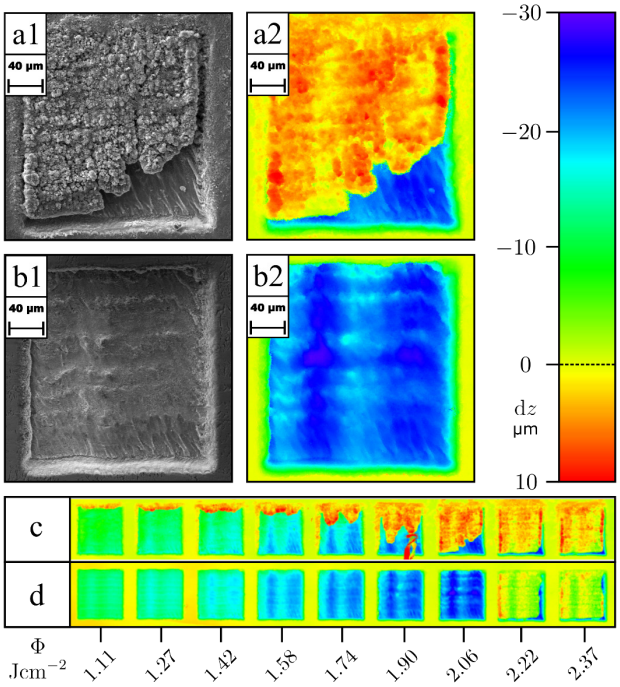

Fig. 6 SEM images (a1, b1) and its corresponding ablation depth dz from a top-viewed 3D-laserscan (a2, b2) of irradiated areas in titanium. Images are both taken directly after processing (a1, a2, c) and after manual post-process cleaning of the same sample with isopropyl alcohol (b1, b2, d). Visual differences after post-process cleaning are attributed to removal of debris and loosely interconnected titanium oxide layers. A constant scanning speed of $\vec{v} = 30$ mm $\mathrm{s^{-1}}$ was used for both variants.

With increasing fluence dose, the irradiated area is gradually covered with a porous layer of titanium oxides. For lower fluence doses, the relatively thin layers already start delaminating from the high pressure of the process gas, which is not the case for a lower gas flow or thicker and therefore mechanically much more resilient layers above $\Phi \approx 2.1$ $\mathrm{Jcm^{-2}}$. Manual post process cleaning was performed by applying a significant amount of pressure on the sample's surface with the help of a cotton stick that was impregnated in isopropyl alcohol. Although this method proved to be effective for shallow surface cleaning and the removal of the loosely interconnected oxide layers, completely encapsulated areas remained unaffected to the greatest extent.

4.2 Ablation – Titanium in water

Focusing high-energy ultrashort laser pulses within a liquid medium is accompanied by various nonlinear phenomena, such as the previously described self-focusing effect and plasma induced breakdown. The threshold

intensity for the latter is mainly depending on the pulse duration, which implies different physical processes for the generation of a high-density plasma, such as multiphoton ionization for femtosecond pulses. Noack et al. used a numerical approach to estimate the laser-induced breakdown in purified water as a function of pulse duration and wavelength [16]. Given by the experimental parameters in this study, an irradiance threshold of approximately $I_{th} = 10^{13}\ \mathrm{Wcm^{-2}}$ can be derived, being about fifty times higher than the maximum achievable pulse intensity. Therefore, even higher ablation rates in water might be possible before laser-induced breakdown obstructs the process. Fig. 7 shows the mean ablation depth $\mathrm{d}z_{avg}$ as a function of fluence Φ and scanning speed $\vec{v}$, similarly to processing within argon, as shown in Fig. 3 beforehand. To maintain comparability between both media, equal process parameters, such as dimensions of the ablation areas, hatching distance, scanning strategy and pulse repetition rate, are also applied for laser ablation in water.

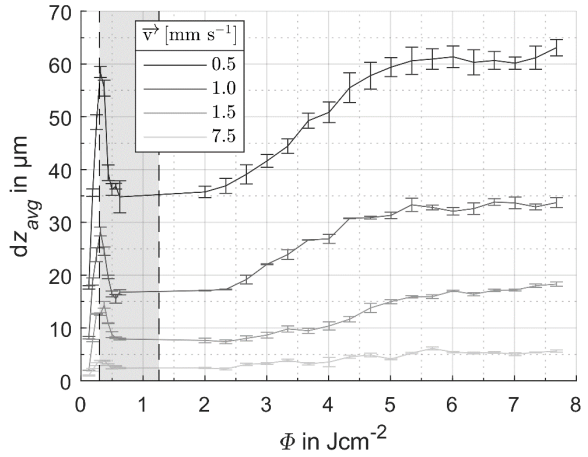

Fig. 7 Average ablation depth $\mathrm{dz_{avg}}$, acquired from laser scanning measurements after laser ablation of titanium under a constant flow of water, as a function of Φ_{pulse} and scanning speed $\vec{v}$. The gray window indicates the range for the expected start of self-focusing within water.

Compared to laser ablation within argon, the required fluence dose to achieve similar ablation depths within water is much higher, which requires a significant reduction in scanning speed within the same fluence range. A simplified explanation in this context is given by the extremely fast cooling rates within the irradiation zone due to a significantly higher thermal conductivity of water and generally impeded debris ejection for denser media. Above the ablation threshold, the rapidly increasing ablation rate has its first maximum located at around $0.25\ \mathrm{Jcm^{-2}}$, independent from the scanning speed. Beyond the first maximum, the declining ablation depth reaches its lowest point at around $1\ \mathrm{Jcm^{-2}}$. Following a much smaller positive gradient, a slightly higher second maximum is observed at around $5-7\ \mathrm{Jcm^{-2}}$, before subsequent saturation is established. A significant influence from self-focusing effects for fluences above the critical threshold of $0.3\ \mathrm{Jcm^{2}}$ is not considered a major driving factor for a second increase in the ablation depth since both maxima are clearly distinguishable even for ablation depths of only a few micrometers. A different, more promising explanation could be given by the fact, that the highly reactive liquid environment, and the confinement of the ablation plume by dense plasma, could promote thermal accumulation effects within surface layers in the ablation zone. It is important to state, that potentially contributing thermal effects are not directly connected to electron excitation during laser irradiation and subsequent lattice thermalization within a few picoseconds. These effects rather result from the temporally separated plasma, with a lifetime of up to several hundred nanoseconds. Although this seems counterintuitively for ultrashort pulsed ablation, accumulative heat conduction for laser ablation in liquids with subsequent melting and / or evaporation may take place at the boundary between surface and ablation plume [17]. For the formation of the two distinctive ablation maxima for laser ablation of titanium in water, two separate mechanisms are supposedly related. For fluences below $1\ \mathrm{Jcm^{-2}}$, fast thermal equilibration between electrons and phonons on a timescale of only a few picoseconds after laser irradiation could be assigned to so called homogenous melting processes near surface layers, while long-lasting heterogeneous melting in deeper layers could be the driving mechanism from spatially confined dense plasma [18]. While those thermally active surface layers cannot be directly held responsible for an increase in ablation depth, they might be an accelerating factor for better material ejection during ablation. Although laser ablation in liquids is subject to many internal physico-chemical processes on timescales from femto- to microseconds whose influence is not fully understood to this date, an adequate approach to describe the mechanisms for ablation of titanium in water can be given by a parameterized variant of Lambert-Beer's law (10).

$$\Delta V = \frac{E_0}{2\Phi}\ln\left(\frac{\Phi}{\Phi_{th,\delta}}\right)\left[\alpha\delta\ln\left(\frac{\Phi}{\Phi_{th,\delta}}\right)+\beta l\ln\left(\frac{\Phi}{\Phi_{th,l}}\right)\right] \qquad (10)$$

The correlation between the fluence Φ and ablation volume ΔV is dependent on the specific material ablation thresholds

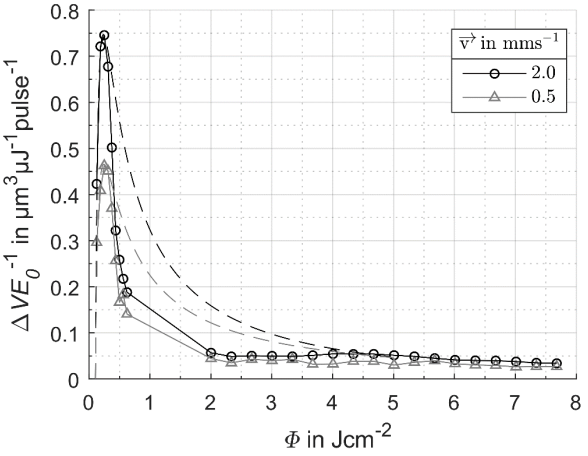

Fig. 8 Specific ablation rates $\Delta V{E_0}^{-1}$, acquired from laser scanning measurements after laser ablation of titanium under a constant flow of water and their respective approximations (dashed lines) according to Lambert Beer´s law, as a function of fluence Φ and scanning speed $\vec{v}$.

$\Phi_{th,i}$ (cf. Fig. 2), optical penetration depths δ, l (cf. (1)), and medium dependent coefficients α, β. Using this model to approximate the specific ablation rate for laser ablation of metals in liquids was successfully demonstration by Kanitz et al. in the investigation for nanoparticle synthesis from iron in different liquid media, such as water, different alcohols, and other solvents [19]. Further examples for machining under gaseous conditions can be found [20, 21]. Fig. 8 exemplarily shows the application of the same principle for titanium in water with their respective specific ablation rates $\Delta V {E_0}^{-1}$, as a function of fluence Φ and different scanning speeds $\vec{v}$. The specific ablation rate describes the process efficiency in terms of energy expense per ablated volume, suggesting an optimal fluence of around 0.25 $\mathrm{Jcm^{-2}}$ with slightly higher ablation rates at higher scanning speeds, supposedly connected to better gas bubble ejection from the ablation zone. However, Fig. 9 demonstrates, that an enhanced temporal efficiency might be achieved for fluences greater than 5 $\mathrm{Jcm^{-2}}$.

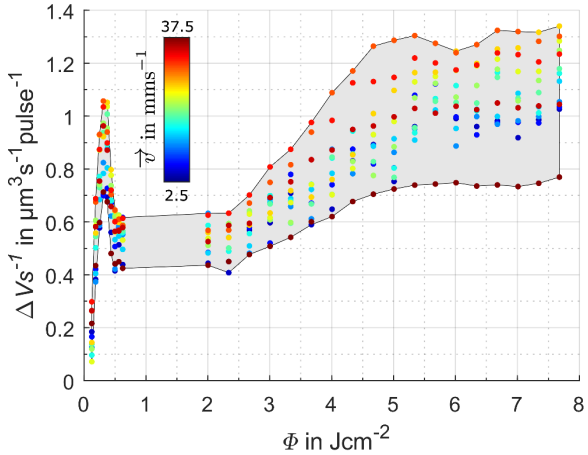

Fig. 9 Volumetric ablation rate for laser ablation of titanium under a constant flow of water, as a function of fluence Φ and scanning speed $\vec{v}$. A first maximum at around 0.25 $\mathrm{Jcm^{-2}}$ is followed by a declining temporal ablation efficiency, before reaching its second maximum within 5 – 7 $\mathrm{Jcm^{-2}}$ with subsequent saturation. On average a slight increase in temporal ablation efficiency for higher scanning speeds is observed at higher fluences, supposedly connected to better gas bubble ejection from the ablation zone.

In contrast to laser ablation in argon, fs-LAL is accompanied by the formation of cavitation bubbles and temporally persistent microbubbles. Although the pulse duration is significantly lower than the time it takes for the initial formation of a single bubble, subsequent laser pulses may hit its expanding boundary layer and undergo various non-intended events, such as deflection and scattering. In this study only for high fluence settings the partially deflected light exceeded the ablation threshold of titanium, which could be observed by slightly affected surfaces beneath ablated zones. While this is considered tolerable, the decreased energy input in the actual ablation zones is impeding the LAL process. To address this issue, opposing scanning and flow directions, high flow rates, and filtering of the persistent microbubbles have successfully been used in this study. Applying static pressure to the fluidic system and using high viscosity liquids may also be a promising approach to further decrease the influence from cavitation bubbles in advanced processing strategies.

Considering the process stability, maintaining a constant fluence to achieve maximum efficiency at the first maximum might be inherently challenging, compared to processing around the second maximum with much shallower adjacent gradients.

4.3 Surface roughness

In addition to different ablation rates between ultrashort pulsed laser ablation of titanium in gaseous environment to laser ablation in liquids, substantial differences in the physicochemical interaction between the hot irradiated matter and the surrounding medium is affecting the near-surface layers in many ways. Most notably, for laser ablation in argon with fluence doses exceeding 12 $\mathrm{kJcm^{-2}}$ a significant increase in surface roughness is observed for increasing quantities of subsequent scanning passes n, as shown in Fig. 10. Contrarily the surface roughness for laser ablation in liquids is decreasing after a fluence dose of 167 $\mathrm{kJcm^{-2}}$, corresponding to the optimal fluence for the first relative ablation rate maximum located at 0.25 $\mathrm{Jcm^{-2}}$ (cf. Fig. 8). For $n > 1$ the specific ablation rate of laser ablation in water only drops insignificantly, while the average surface roughness is lower than compared to argon.

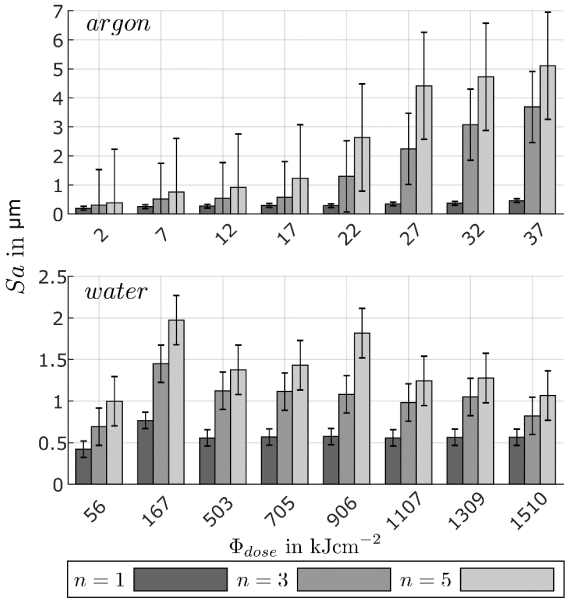

Fig. 10 Average surface roughness, acquired from laser scanning measurements after laser ablation of titanium under a constant flow of argon and under a constant flow of water, as a function of different fluence doses Φ_{dose} and quantity of subsequent scanning passes n. Scanning speeds $\vec{v}$ for argon (90 $\mathrm{mms^{-1}}$) and water (4 $\mathrm{mms^{-1}}$) were specifically chosen, so that roughness values with similar corresponding maximum volumetric ablation rates are compared.

Additional tests with extremely low scanning speeds of just 0.5 $\mathrm{mms^{-1}}$ resulted in the complete penetration of the 125 µm thick titanium foil for a single pass, due to a massive increase in the applied fluence dose. However, the excessive formation of gas bubbles deflecting the laser beam presumably compromised the surface quality of adjacent regions at a larger scale than compared to an increased count of subsequent ablation passes and a similar processing time. Thus, multiple passes with higher scanning speeds should be

preferred over a single pass with lower scanning speed to achieve adequate surface qualities. Surface changes for both processes and at different fluence doses are visually represented by SEM images in Fig. 11. For laser ablation within argon at low fluence doses, laser-induced periodic surface structures (LIPSS) can be observed (a1), similar to processing within vacuum [1] and water [22]. At higher fluence doses, the surface quality is compromised by poor dimensional tolerances at the edges, excessive formation of layers consisting of titanium oxides, and surface contamination of recondensed particles (a2).

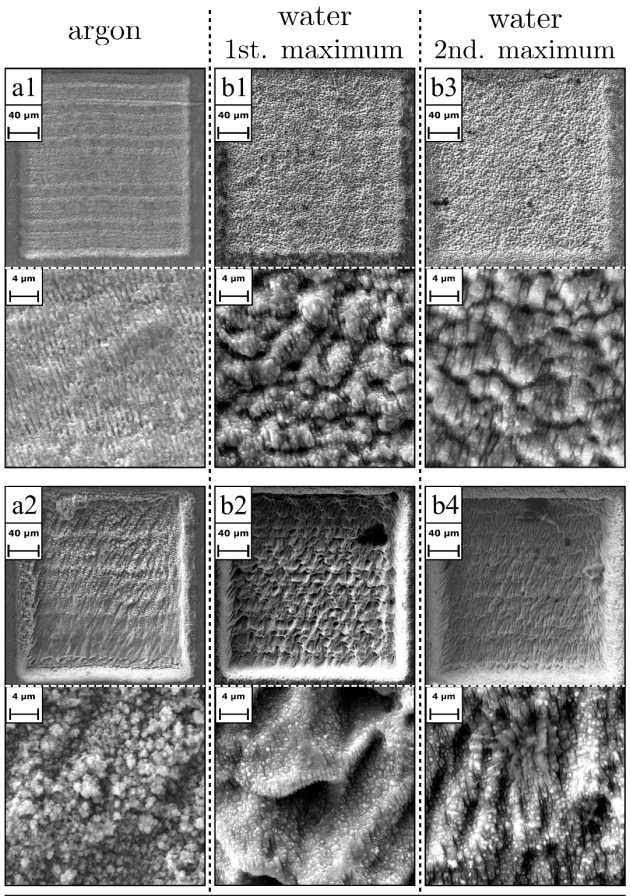

	a1	a2	b1	b2	b3	b4
dz µm²	4.7	25.8	2.2	47.6	4.3	59.3
Φ_{dose} kJcm^{-2}	10	77	60	893	805	12080

Fig. 11 SEM images taken from irradiated titanium after laser ablation under a constant flow of argon (a1, a2) and after laser ablation under a constant flow of water at two distinctive ablation maxima (b1, b2) and (b3, b4). The upper six images correspond to fluence doses Φ_{dose} near the ablation threshold, while the values for the lower six images are 7.5 times higher for argon and 13.5 times higher for water. At low fluence doses, higher surface roughness is observed for processing within water. For processing at higher fluence doses (a2), excessive formation of titanium oxides reduces surface quality, especially for processing within argon. For processing within water near the second maximum (b4), the surface roughness is lowered substantially, while simultaneously requiring a much larger fluence dose than for the first maximum (b2).

For laser ablation within water at low fluences the surface structures for both maxima are visually similar, although the fluence dose for the second maximum is more than 13 times higher. Both surfaces show an irregular arrangement with little signs of recondensed debris (b1, b3). Further increase of the fluence doses through lower scanning speeds while simultaneously maintaining the same fluences reveals distinguishable changes to the surface structures (b2, b4). While at the first maximum large irregular structures with large amplitudes are visible, increased fluence doses at the second maximum supposedly lower their magnitude and in turn the surface roughness. Regarding ablation within water, the differentiation between ablation near the first (b1, b2) and second (b3, b4) maximum reveals a significant improvement in terms of surface roughness at the expense of significantly higher fluence doses required for comparable ablation depths dz.

5. Conclusion

In this study, the impact of argon and purified water on the process efficiency and surface quality for femtosecond laser ablation of thin metal foils, made from grade 1 titanium, is investigated. For both processes, in-focus laser ablation of the titanium surface was performed under comparable experimental conditions. Acquisition of laser scanning measurements shown in this study was obtained from three subsequent measurements at different positions in the ablation zones of two separate experiments in argon and water respectively. SEM images were taken after laser scanning to preserve the integrity of the samples. Comparative measurements from previous experiments were almost identical. For processing in water, linear absorption and nonlinear self-focusing effects were considered.

For fluence doses below $35\ \mathrm{kJcm^{-2}}$, a logarithmic ablation characteristic could be assigned to processing under a constant flow of argon, irrespective of different combinations of fluence and scanning speed. Beyond that threshold, gradual formation of ceramic surface layers made from titanium oxides is reported with increasing fluence dose. Investigations of delaminated oxide layers with SEM and laser scanning microscopy revealed free-floating structures with large voids underneath. A possible explanation is given by plasma-induced defocusing above the surface and subsequent self-focusing of the laser beam within the semi-transparent ceramic structures, inducing sub-surface ablation and expansion of the porous oxide layers. Stating that those observations took place under argon, an insufficient turbulent flow characteristic with presence of atmospheric oxygen can be held responsible for this effect.

Laser ablation of titanium within purified water revealed two separate ablation maxima, with almost identical magnitude. The first ablation maximum is located at a fluence of around $0.25\ \mathrm{Jcm^{-2}}$ close to the specific ablation threshold for titanium and can be assigned to the same excitation processes as for ablation within argon. Between the first and the second maximum at around $5-7\ \mathrm{Jcm^{-2}}$, plasma-shielding supposedly lowers the ablation efficiency, before accumulative effects from confined plasma and high pressures become relevant and increase the ablation rate again. Although much slower in terms of volumetric ablation rate, a significant improvement of the dimensional tolerances and surface-quality in terms of roughness and surface contamination by recondensed debris could be observed for laser ablation in liquids. This makes the process

a promising alternative for micromachining without the need of excessive post-processing.

Acknowledgments

This project was supported by the Federal Ministry of Economic Affairs and Climate Action (IGF project no.: 21971N)

References

[1] M. Tsukamoto, T. Kayahara, H. Nakano, M. Hashida, M. Katto, M. Fujita, M. Tanaka, and N. Abe: J. Phys., 59, (2007) 666.

[2] S. Nolte, C. Momma, H. Jacobs, A. Tünnermann, B. N. Chichkov, B. Wellegehausen, and H. Welling: J. Opt. Soc. Am. B, 14, (1997) 2716.

[3] J. Ren, M. Kelly, and L. Hesselink: Opt. Lett., 30, (2005) 1740.

[4] P. Maack, A. Kanitz, J. Hoppius, J. Köhler, C. Esen, and A. Ostendorf: Proc. SPIE, (2022) 119890L.

[5] A. Garcia-Giron, D. Sola, and J. I. Peña: Appl. Surf. Sci, 363, (2016) 548.

[6] J. Neddersen, G. Chumanov, and T. M. Cotton: Appl. Spectrosc., 47, (1993) 1959.

[7] M. V. Shugaev, C. Wu, O. Armbruster, A. Naghilou, N. Brouwer, D. S. Ivanov, T. J.-Y. Derrien, N. M. Bulgakova, W. Kautek, B. Rethfeld, and L. V. Zhigilei: MRS Bull., 41, (2016) 960.

[8] V. M. Tabie, M. O. Koranteng, A. Yunus, and F. Kuuyine: Lasers Manuf. Mater. Process., 6, (2019) 189.

[9] V. Tangwarodomnukun, P. Likhitangsuwat, O. Tevinpibanphan, and C. Dumkum: Int. J. Mach. Tools Manuf., 89, (2015) 14.

[10] G. M. Hale and M. R. Querry: Appl. Opt., 12, (1973) 555.

[11] J. M. Liu: Opt. Lett., 7, (1982) 196.

[12] E. Nibbering, M. A. Franco, B. S. Prade, G. Grillon, C. Le Blanc, and A. Mysyrowicz: Opt. Commun., 119, (1995) 479.

[13] G. Schnell, U. Duenow, and H. Seitz: Materials, 13, (2020) 969.

[14] A. J. Antończak, B. Stępak, P. E. Kozioł, and K. M. Abramski: Appl. Phys. A, 115, (2014) 1003.

[15] F. Kiel, N. M. Bulgakova, A. Ostendorf, and E. L. Gurevich: Phys. Rev. Appl., 11, (2019) 024038.

[16] J. Noack and A. Vogel: IEEE J. Quantum Electron., 35, (1999) 1156.

[17] A. Kanitz, M.-R. Kalus, E. L. Gurevich, A. Ostendorf, S. Barcikowski, and D. Amans: Plasma Sources Sci. Technol., 28, (2019) 103001.

[18] M. Z. Mo, Z. Chen, R. K. Li, M. Dunning, B. B. L. Witte, J. K. Baldwin, L. B. Fletcher, J. B. Kim, A. Ng, R. Redmer, A. H. Reid, P. Shekhar, X. Z. Shen, M. Shen, K. Sokolowski-Tinten, Y. Y. Tsui, Y. Q. Wang, Q. Zheng, X. J. Wang, and S. H. Glenzer: Science, 360, (2018) 1451.

[19] A. Kanitz, J. S. Hoppius, M. Fiebrandt, P. Awakowicz, C. Esen, A. Ostendorf, and E. L. Gurevich: Appl. Phys. A, 123, (2017) 674.

[20] B. Neuenschwander, B. Jaeggi, M. Schmid, and G. Hennig: Physics Procedia, 56, (2014) 1047.

[21] T. Kramer: J. Laser Micro/Nanoeng., 12, (2017) 107.

[22] C. Albu, A. Dinescu, M. Filipescu, M. Ulmeanu, and M. Zamfirescu: Appl. Surf. Sci., 278, (2013) 347.

(Received: July 4, 2023, Accepted: December 10, 2023)